ISSN No:-2456-2165 https://doi.org/10.38124/ijisrt/26may1953

Investigation of Steering Angle Influence on the Velocities of Four Independently Driven Wheels for a Mobile Robot

Le Quoc Chuan[1]; Pham Quoc Phong[1*]; Thach Minh Trong[1]

[1]College of Engineering and Technology, Tra Vinh University, Vinh Long, Vietnam

Corresponding Author: Pham Quoc Phong[*]

Publication Date: 2026/06/05

Abstract: Independent velocity coordination at each wheel is a key factor in governing the kinematics and trajectory control of omnidirectional mobile robot configurations. This study investigates the design and experimental validation of an electronic differential system that distributes reference velocities based on the steering input for a four-wheel independent steering and four-wheel independent drive mobile robot. Utilizing the geometric principles of an expanded Ackermann steering model, an inverse kinematic framework is established to map the mathematical constraints between the global linear velocity and localized steering angles, aiming to minimize geometric synchronization mismatches during cornering maneuvers. For the physical validation, a mechatronic prototype intended for baseline algorithm verification was constructed, integrating an Arduino Mega microcontroller, self-locking worm-gear steering mechanisms, and brushless direct current hub motors regulated by four independent drives. To isolate the core actuation performance from stochastic ground-interaction variables, a no-load bench-testing configuration was utilized. The comparative analysis between the MATLAB/Simulink numerical simulation and the empirical sensor data demonstrates that the isolated wheel velocity control loops track the distributed kinematic references effectively, maintaining a steady-state velocity tracking error below 5% across most investigated cornering profiles. The findings provide a foundational reference and a reliable hardware verification framework for developing autonomous guided vehicles tailored for agricultural monitoring, cultivation, and complex industrial environments.

Keywords: *Mobile Robot; Brushless DC Motor; Electronic Differential System; Four-Wheel Independent Drive; MATLAB/Simulink.*

How to Cite: Le Quoc Chuan; Pham Quoc Phong; Thach Minh Trong (2026) Investigation of Steering Angle Influence on the Velocities of Four Independently Driven Wheels for a Mobile Robot. *International Journal of Innovative Science and Research Technology*, 11(5), 3282-3290. https://doi.org/10.38124/ijisrt/26may1953

I. INTRODUCTION

In the advancing landscape of automation, deploying mobile robotic systems within industrial logistics and high-tech agricultural sectors introduces rigorous challenges regarding structural maneuverability, spatial positioning accuracy, and operational stability across confined spaces or variable terrains. Specifically, the development of autonomous guided vehicles designed for agricultural monitoring and cultivation assistance demands exceptional locomotive flexibility. To address these mobility requirements, a four-wheel independent steering and four-wheel independent drive architectural configuration represents a highly viable engineering approach. By equipping each wheel assembly with dedicated steering and traction actuators, this configuration enables the robot to execute highly flexible trajectories, including parallel crab steering or zero-radius turning, which are fundamentally unachievable using conventional mechanical differential linkages [1, 2].

However, managing multiple coupled degrees of freedom simultaneously on this platform necessitates solving complex kinematic and dynamic coordination problems. Realtime operations mandate continuous synchronization between the individual steering angle and the corresponding angular velocity of each wheel. Geometric discrepancies among the decoupled wheels, if not appropriately regulated, inevitably result in forced lateral tyre scrubbing or structural fighting, which increases energy consumption, accelerates tyre wear, and degrades overall path-following accuracy [3,4]. To alleviate these structural inconsistencies, an electronic differential system is typically developed, requiring an accurate mathematical mapping model combined with feedback control loops to compensate for the localized non-linearities of the hardware components [5].

ISSN No:-2456-2165 https://doi.org/10.38124/ijisrt/26may1953

II. LITERATURE REVIEW

In relevant literature, various control methodologies have been proposed to enhance trajectory tracking, ranging from differential geometry formulations and finely tuned PID topologies to Fuzzy Logic and Artificial Neural Network adaptations [6–8]. Nonetheless, a significant portion of current research remains restricted to traditional two-wheel differential drive robots or synchronous mechanical drive assemblies. Detailed investigations into the real-time coordination between steering commands and physical wheel velocities on decentralized mechatronic prototypes require further empirical validation to explicitly clarify the influence of hardware latencies and mechanical compliance.

Motivated by these operational demands, particularly the objective of advancing autonomous mobile platforms for agricultural monitoring and crop cultivation, this study establishes a kinematic mathematical model, develops a numerical simulation framework, and implements a baseline bench-test evaluation of a dedicated mobile robot prototype. The electronic differential algorithm is structured upon an expanded Ackermann geometric principle within the MATLAB/Simulink environment and subsequently embedded into the physical microcontroller hardware. Through distinct steering profiles executed under controlled laboratory bench conditions, the velocity distribution responsiveness and actuation synchronization are quantified. The resulting insights aim to contribute useful design baselines for constructing highly maneuverable robotic platforms in agricultural and industrial sectors.

III. RESEARCH METHODS

➢ *Mechanical Configuration*

The structural chassis of the mobile robot was constructed using industrial-grade 30 × 30 mm aluminum extrusions, securely assembled via right-angle bracket gussets and hexcap fasteners to minimize structural vibrations. The chassis frame is reinforced with an engineered plywood deck measuring 800 × 600 × 10 mm, which provides a rigid housing surface for the onboard electronic control boards and power management units.

The integrated physical architecture and the multi-degree-of-freedom decoupled wheel assemblies are illustrated in Fig.1. The directional steering system utilizes individual stepper motors coupled with a high-ratio worm-gear transmission. The inherent mechanical selflocking characteristic of the worm-gear arrangement maintains stable steering angles against external ground disturbances, thereby reducing the continuous holding current required by the stepper motor windings and enhancing energy efficiency. The primary traction drive utilizes direct-drive brushless direct current Hub Motors embedded within the wheel rims, regulated by four independent power driver modules featuring H-bridge MOSFET layouts with a 400 W power margin to prevent instantaneous voltage drops during rapid velocity transitions.

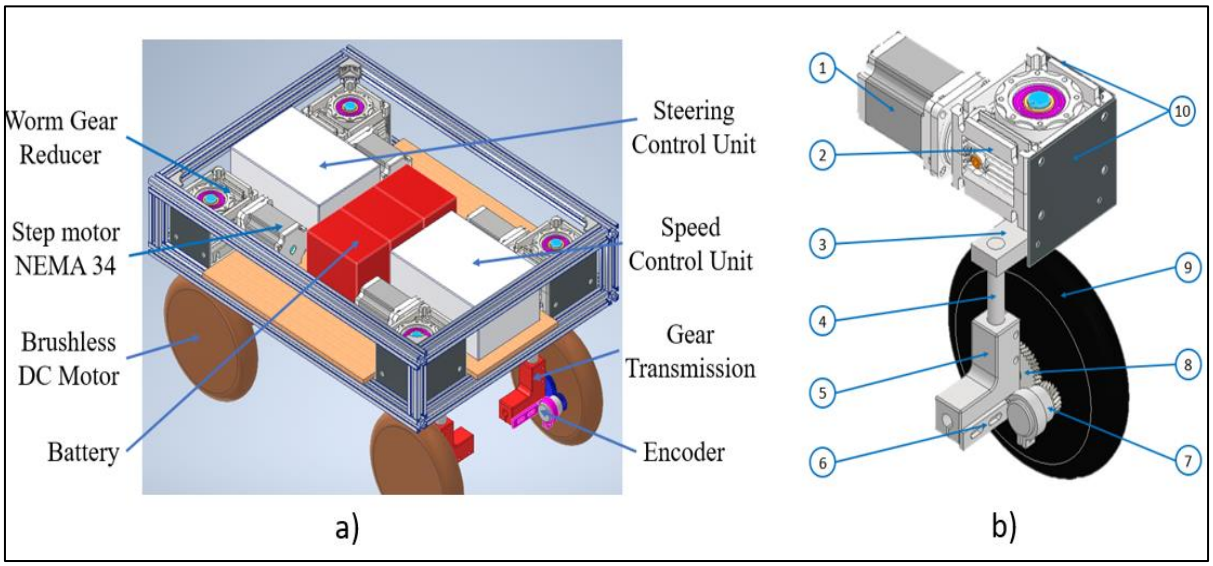

Fig 1 Mechanical Layout of the System: (a) Overall 3D Rendering of the Robot Platform, (b) Detailed Structural Composition of the Decoupled Wheel Module

As depicted in Fig. 1b, the structural assembly of each independent wheel module combines computer numerical control (CNC) machined parts and high-density 3D-printed elements, structurally tied through ten core components. The entire sub-assembly is rigidly integrated with the primary chassis (Fig. 1a) via an engineered mounting flange (10). Directional actuation is delivered by a Nema 86 stepper motor (1) driving a worm-and-gear reducer with a 1:15 reduction ratio (2). This mechanism transfers rotational torque down to a central shaft (4) via a directional linkage bar (3), pivoting the wheel yoke housing (5) to adjust the local steering angle based on control inputs.

To capture the actual rotational velocity, an optical quadrature encoder (7) is positioned on a dedicated sensor mount (6). The angular rotation from the wheel assembly housing the Hub Motor (9) is transmitted to the encoder shaft through a spur gear train with a 1:2 speedup ratio (8). This mechanical configuration is specifically selected to guarantee mechanical stiffness under structural loads while minimizing

ISSN No:-2456-2165 https://doi.org/10.38124/ijisrt/26may1953

backlash inside the sensor feedback loop during active operations.

To drive the physical actuators described in Fig. 1b, the primary electronic hardware is arranged as a centralized, modular layout on a main chassis panel, as shown in Fig. 2. This electrical configuration coordinates power distribution and digital signals to achieve synchronization between the steering trajectories and localized wheel velocities. An Arduino Mega microprocessing board is programmed to receive directional navigation commands, compute the inverse kinematic expressions of the algorithm, and transmit the appropriate control signals to the power drivers.

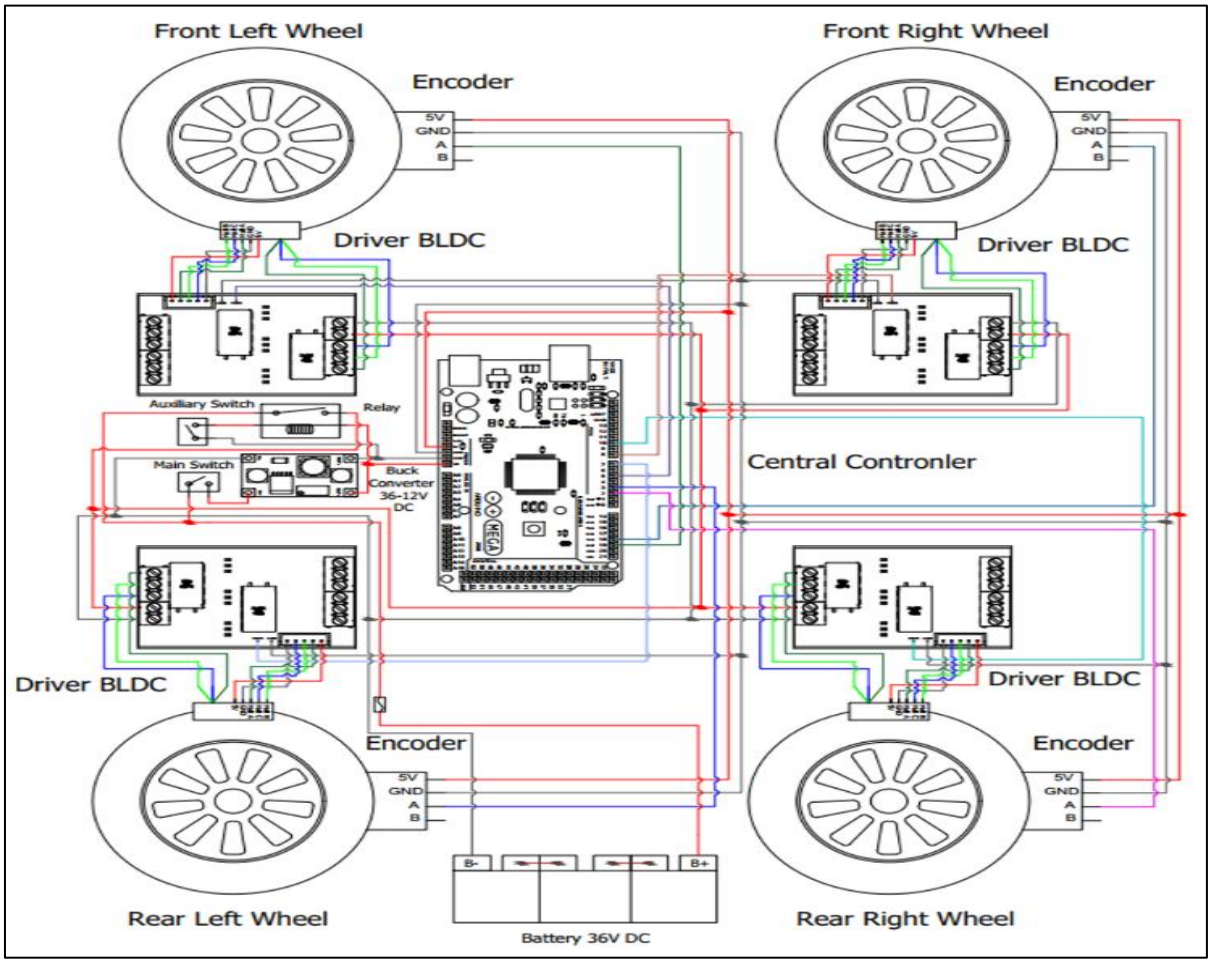

Fig 2 Electrical Wiring Layout of the Robot Control System

The kinematic correlation and closed-loop signal processing between the electrical system (Fig. 2) and the wheel hardware assemblies (Fig. 1b) are executed via three primary streams: the steering control stream routes command pulses from the Arduino Mega through driver units to the Nema 86 stepper motors and 1:15 worm gear reducers to establish the steering angles; the velocity control stream delivers PWM signals from the algorithm to the four drivers to modulate the Hub motor speeds; and the kinematic feedback loop feeds quadrature signals from the optical encoders (via a 1:2 gear ratio) back to the external interrupt pins of the microcontroller for discrete-time PID regulation.

➢ *Control Architecture*

The central processing architecture of the mobile platform is deployed on an Arduino Mega microcontroller board, programmed using native C/C++ structures. Fig. 2 details the structural interconnects of the control panel, where each independent motor speed controller interfaces directly with a dedicated hardware PWM channel on the Arduino board.

The localized velocity of each driven wheel is recorded by an optical quadrature encoder generating 600 pulses per revolution (ppr), which are fed back to the processing unit. The captured pulse frequency is processed through internal algorithms to compute the actual wheel linear speed. The centralized Arduino Mega board continuously calculates the tracking error between the theoretical reference velocity generated by the mapping and the empirical feedback velocity, executing discrete-time PID control loops to output corrected command signals to the respective motor drives.

➢ *Electronic Differential Formulation*

The structural deployment of a four-wheel independent drive platform, where each individual wheel is actuated by a decoupled motor capable of independent speed and torque modulation, requires strict geometric coordination among the active wheels to ensure predictable motion paths and vehicle

ISSN No:-2456-2165 https://doi.org/10.38124/ijisrt/26may1953

stability [9, 10]. Under low-speed operating regimes and constrained steering conditions, the maneuvering configuration shown in Fig. 3 is evaluated (where the two front wheels pivot toward the intended direction of travel and the two rear wheels pivot symmetrically in the opposite direction) to minimize the turning radius and maximize spatial agility within narrow zones. For transitions at higher linear velocities, the tracking scenario outlined in Fig. 4 (where all four wheels pivot in a parallel direction) can be deployed to enable rapid lateral lane shifts while minimizing structural yaw instability and obstacle collision risks.

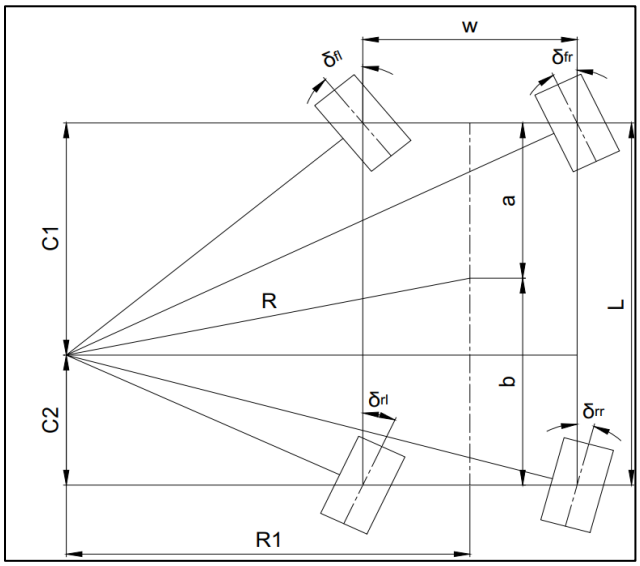

Fig 3 Geometric Schematic for Low-Speed Maneuvering Mode

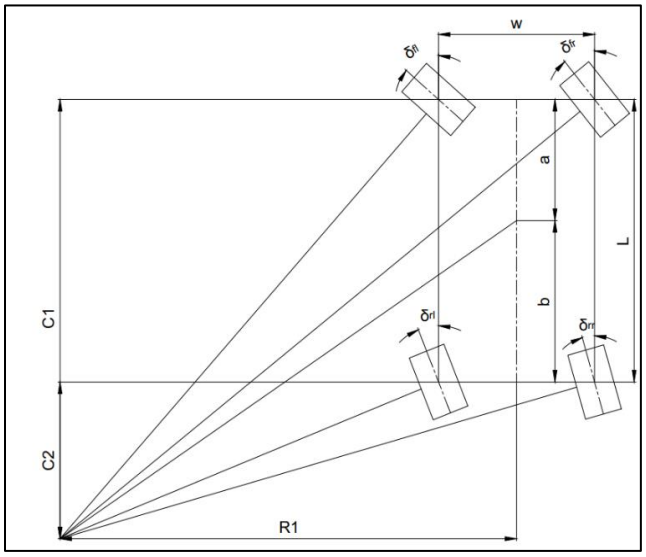

Fig 4 Geometric Schematic for High-Speed Maneuvering Mode

Based on the geometric constraints established for the low-speed operating regime (with a baseline nominal velocity V = 2.778 m/s), the turning center parameters and instantaneous turning radius R_1 are integrated into a single formulation layout in equation (1):

$$C_1 = \frac{L.c}{1+c},\ C_2 = L - C_1,\ R_1 = \frac{C_1}{\tan(\delta_{front})} \quad (1)$$

$$\left(where\ c = \frac{\tan(\delta_{front})}{\tan(\delta_{rear})}\right)$$

From the calculated global Instantaneous Center of Rotation (ICR), the localized steering angles assigned to the four individual steering actuators (fl: front-left, fr: front-right, rl: rear-left, rr: rear-right) are derived via inverse trigonometric functions in equation (2). This mathematical mapping represents a pure kinematic steering assumption designed to maintain the wheel planes perpendicular to their respective geometric radii drawn from the ICR:

$$\begin{cases} \delta_{fl,fr} = arctan\left(\frac{C_1}{R_1 \mp \frac{W}{2}}\right) \\ \delta_{rl,rr} = -\ arctan\left(\frac{C_2}{R_1 \mp \frac{W}{2}}\right) \end{cases} \quad (2)$$

Concurrently, the specific turning radii measured from the ICR point to the axle centers and individual ground-contact patches are compacted into the combined system expression in equation (3):

$$\begin{cases} R_{front} = \frac{C_1}{\sin(\delta_{front})}, & R_{rear} = \frac{C_2}{\sin(\delta_{rear})} \\ R_{fl,fr} = \frac{C_1}{\sin(\delta_{fl,fr})}, & R_{rl,rr} = \frac{C_2}{\sin(\delta_{rl,rr})} \end{cases} \quad (3)$$

Finally, the electronic differential system algorithm incorporates these localized geometric radii values to calculate the theoretical reference angular velocities (ω_i, where i $\in$ {*fl, fr,rl,rr*}) mapped to the individual motor drives according to the integrated inverse kinematic system outlined in (4):

$$\begin{cases} \omega_{fl,fr} = \omega.\frac{R_{fl,fr}.\delta_{fl,fr}}{R_{front}.\delta_{front}} \\ \omega_{rl,rr} = \omega.\frac{R_{rl,rr}.\delta_{rl,rr}}{R_{rear}.\delta_{rear}} \end{cases} \quad (4)$$

Within the mathematical framework of equations (1) to (4), the geometric and kinematic variables correlate directly with the analytical schematics (Fig. 3, Fig. 4) and the hardware dimensions (Table 1) as follows: L and W represent the wheel-base and track-width of the robot platform, respectively; δ_{front} and δ_{rear} define the nominal steering angles at the front and rear axle centers, which determine the global position of the ICR; C_1 and C_2 are the longitudinal distances from the axle lines to the projected ICR axis; and R_1 is the turning radius of the geometric center of the robot. For each decoupled wheel module (indexed by i $\in$ {*fl, fr,rl,rr*} denoting front-left, front-right, rear-left, and rear-right), δ_i and R_i signify the localized steering angle and the theoretical kinematic turning radius, designed to align the tyre plane perpendicularly to the ICR vector. Lastly, ω is the angular velocity of the main vehicle frame, while ω_i constitutes the target reference angular velocity commanded to each Hub Motor to maintain deterministic trajectory mapping under zero-slip assumptions.

ISSN No:-2456-2165 https://doi.org/10.38124/ijisrt/26may1953

For the numerical simulation environment, independent PID structures are developed alongside synthesized steering command trajectories to generate target steering profiles while the target linear velocity is maintained at a constant value. These command streams, combined with the structural dimensions of the platform, are processed within the MATLAB Function 1 block to calculate the geometric steering angles for each wheel. The localized velocity distribution block, programmed inside the MATLAB Function 2 block, receives these calculated steering angles and the target global velocity to map out the corresponding reference speeds for each wheel across the evaluated maneuver profiles [11].

➢ *Matlab/Simulink Modeling*

The numerical simulation model of the independent four-wheel drive system was developed within the MATLAB/Simulink environment, structured around core functional elements: standard PID Controller blocks, custom MATLAB Function blocks, a Signal Builder block for profile generation, Transfer Fnc blocks modeling actuator dynamics, and dedicated signal routing and acquisition blocks.

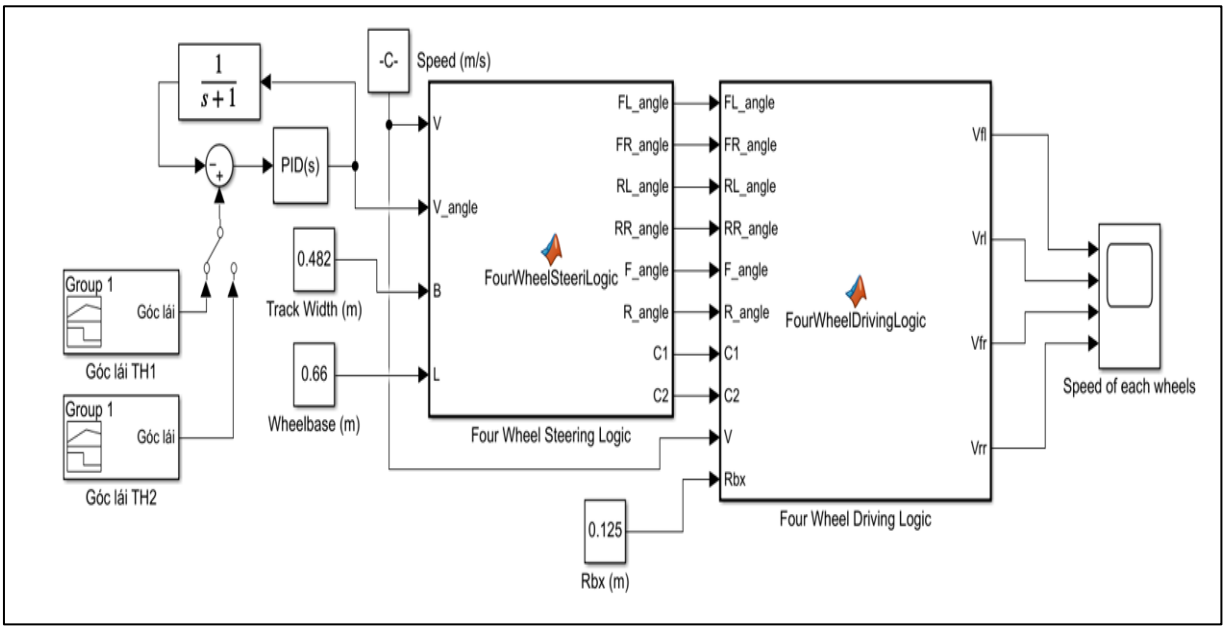

Fig 5 Block Diagram of the Four-Wheel Independent Drive System Simulation in MATLAB

➢ *Experimental Setup*

To perform initial mechatronic verification and quantify the baseline tracking loop performance of the physical hardware, an experimental routing layout and test bench structure were arranged as illustrated in Fig. 6. To clearly document the physical parameters of the mobile prototype used during these laboratory trials, the specifications of the core mechatronic components are compiled in Table 1.

Based on the structural configuration detailed in Table 1, the core geometric parameters including a wheel-base L = 0.5 m, a track-width W = 0.44 m, and a nominal wheel radius R_w = 0.065 m were selected to match the physical parameters defined in the mathematical equations and the MATLAB/Simulink numerical environment. Maintaining identical pa-rameter fields ensures that the embedded inverse kinematic matrix accurately maps the target relationships between the steering angles δ and the target linear velocity V, minimizing model-induced discrepancies during baseline operations.

Regarding the real-time control flow and data logging structure illustrated in Fig. 6, the system operates as a closed-loop architecture. The centralized Arduino Mega board acts as the primary processing node, receiving the pre-programmed maneuver profiles, executing the inverse kinematic calculations of the Ackermann-based algorithm, and generating the necessary actuation commands.

Table 1 Mechatronic Component Specifications of Robot

Hardware Component	**Technical Parameter / Attribute**
Central Processing	Arduino Mega
Traction Actuators	4×Hub Motors 300 W
Drivers	4×H-Bridge MOSFET, 400 W
Steering Actuators	4×Nema 86 Stepper Motors
Transmission Mechanism	Worm-and-Gear (1:15 Ratio)
Feedback Sensors	Encoders (600 ppr resolution)
Power Storage System	3 × DC Lead-Acid Batteries
Chassis Dimensions	L = 0.5 m; W = 0.44 m

ISSN No:-2456-2165 https://doi.org/10.38124/ijisrt/26may1953

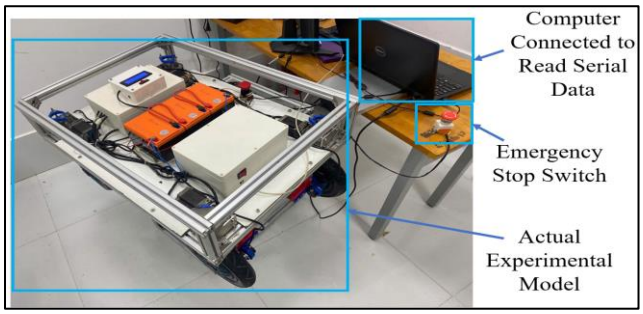

Fig 6 Schematic of the Experiment Setup and Real-Time Data Logging Stream

For the steering system, the four Nema 86 stepper motors coupled with the 1:15 wormgear transmissions maintain the targeted steering angles δ securely against external mechanical feedback due to the non-reversible, self-locking nature of the worm assembly.

For the traction drive loops, the localized velocity reference commands are converted into high-frequency PWM outputs and transmitted to the four independent power driver modules, which regulate the four 300 W Hub Motors. To isolate the primary actuation control loops from complex tyre-road friction dynamics and stochastic slipping, the robot chassis was mounted on a rigid stationary test bench for these baseline trials. This no-load experimental configuration permits direct evaluation of the deterministic velocity mapping generated by the algorithm and quantifies the tracking bandwidth of the hardware independent of terrain variables. The feedback loop utilizes four optical encoders (600 ppr) mounted coaxially with the wheel hubs. The actual rotational velocities (V_{fl},V_{fr},V_{rl},V_{rr}) are captured, filtered via digital low-pass smoothing routines, and routed back to the Arduino PID loops to correct tracking errors while simultaneously being transmitted to a host PC via UART serial communication for synchronous logging and comparative analysis.

IV. RESULTS AND DISCUSSION

➢ *Simulation Results*

Numerical simulations were conducted over a 12-second window to evaluate the kinematic coordination of the electronic differential system (EDS) across distinct steering trajectories, namely a simulated roundabout traversal (Case 2) and a continuous periodic weaving profile (Case 3), as shown in Fig. 7. The corresponding individual wheel linear velocities computed within the simulation environment are plotted in Fig. 8 and Fig. 9.

For Case 2 (Fig. 8), the onset of a left-hand turn induces a proportional deceleration at the inner wheels (front-left and rear-left to 2.768 m/s and 2.763 m/s, respectively), while the outer wheels accelerate (front-right and rear-right to 2.796 m/s and 2.804 m/s, respectively). This distribution reverses symmetrically during right-hand maneuvers, with all curves intersecting precisely at the baseline linear speed of 2.778 m/s during straight-line transitions ($t \in [0,2]$ s and $t \in [10,12]$ s). This behavior validates the geometric consistency of the inverse kinematic mapping under zero-steering constraints.

In Case 3 (Fig. 9), the periodic steering input varies with an increasing angular amplitude from 5^o to 30^o. The velocity divergence between the inner and outer paths scales linearly with the steering amplitude, expanding from a negligible 0.002 m/s at 5^o to a maximum of 0.254 m/s at a peak angle of 30^o. The smooth, non-oscillatory velocity transitions without discontinuities confirm the numeric stability and transient reliability of the underlying mathematical model under highly dynamic inputs.

➢ *Experimental Results*

To validate the real-time tracking performance of the physical prototype, no-load laboratory bench tests were executed on a stationary support frame, isolating the mechatronic actuation loops from stochastic tire-road interactions. The empirical data recorded via the quadrature encoders are consolidated and compared against the numerical simulation references in Table 2, with the continuous time-domain trajectories visualized in Fig. 10.

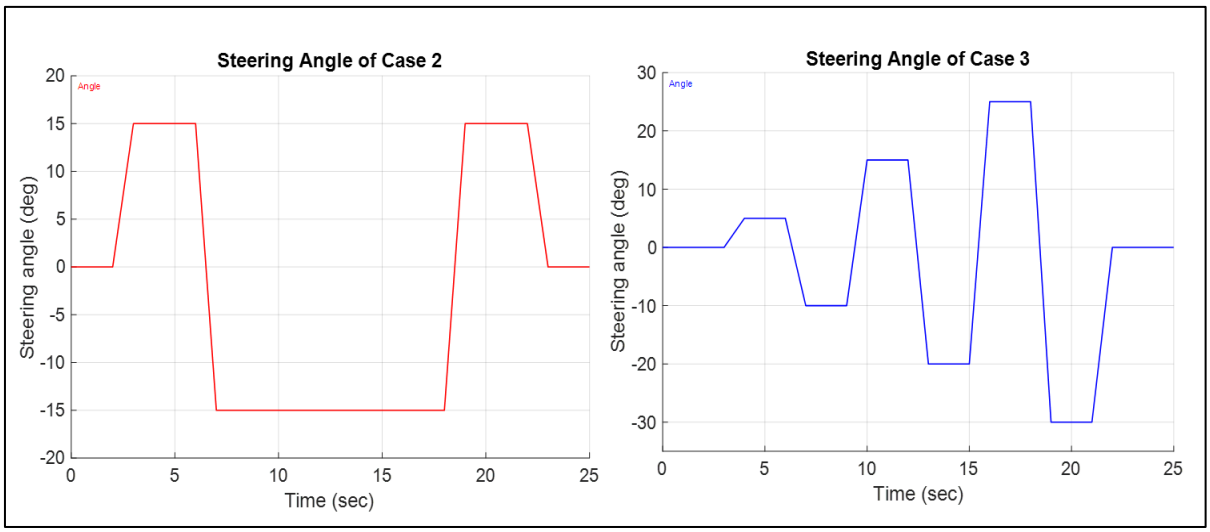

Fig 7 Target Steering Command Profiles Evaluated Over the Simulation Timeline

ISSN No:-2456-2165 https://doi.org/10.38124/ijisrt/26may1953

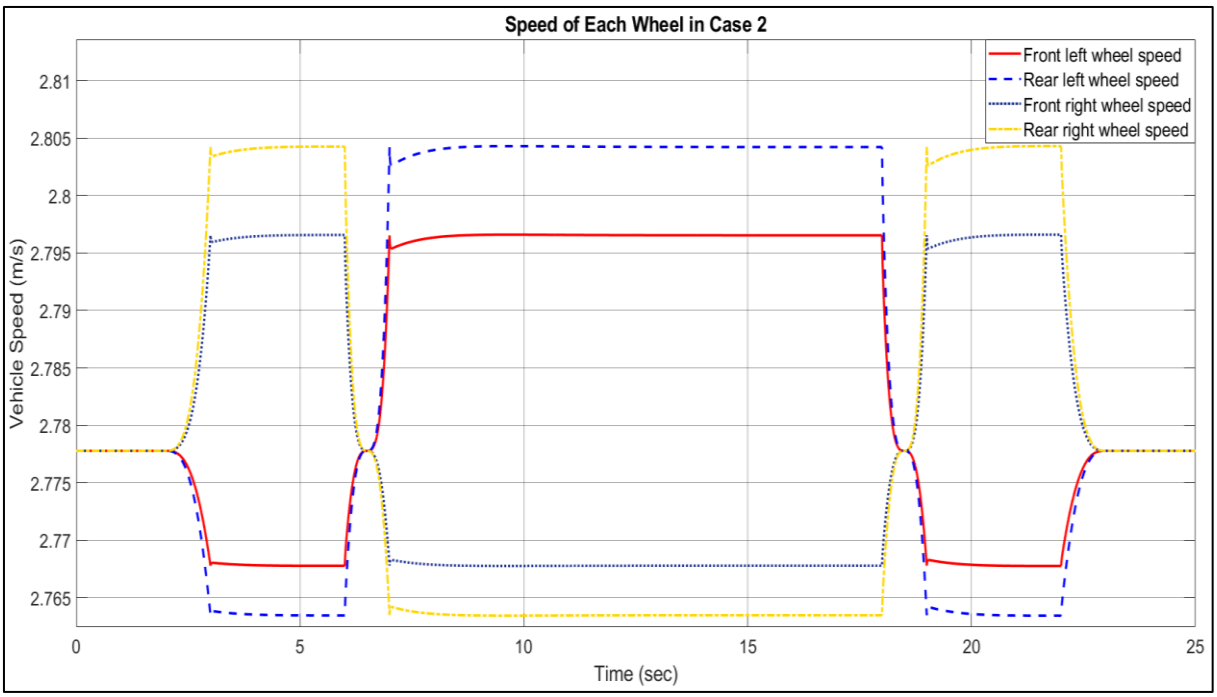

Fig 8 Distributed Individual Wheel Velocities Simulated Under Case 2 Conditions

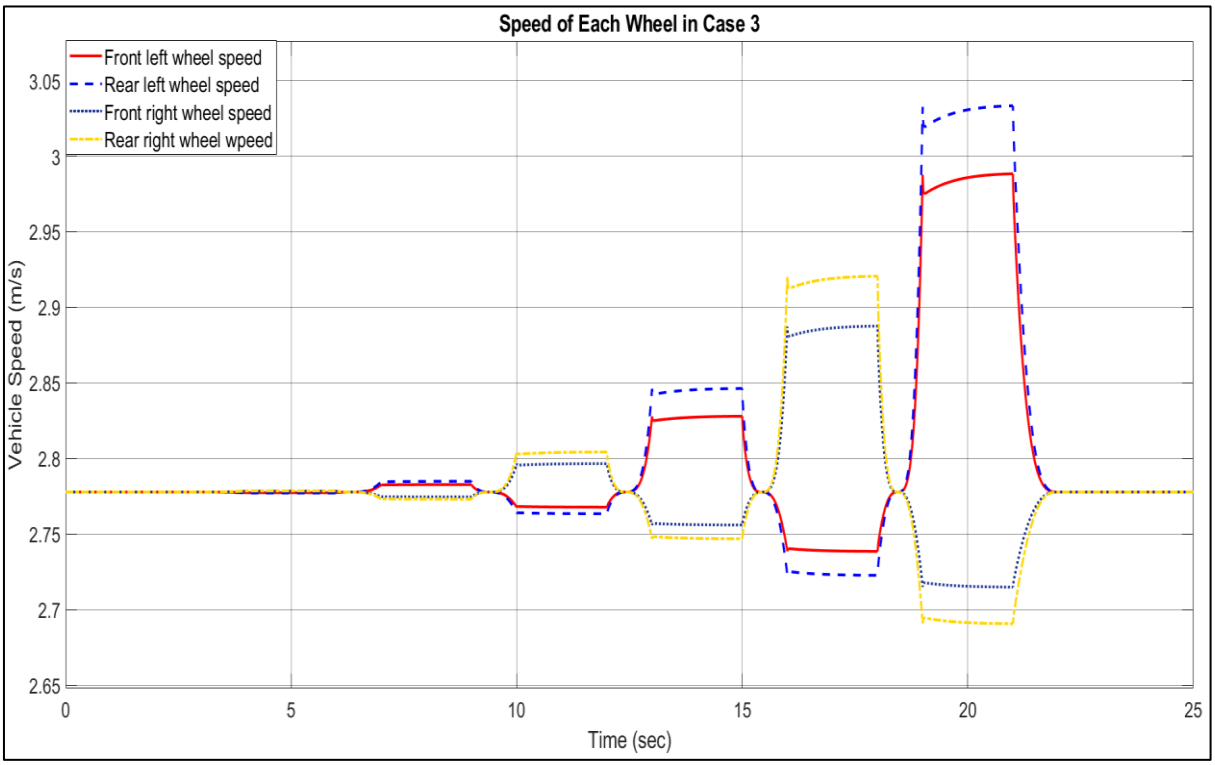

Fig 9 Distributed Individual Wheel Velocities Simulated Under Case 3 Conditions

Table 2 Data of Individual Wheel Velocities Between Simulation and Experiment

Scenario	t (s)	δ (◦)	Source	V_{fl} (m/s)	V_{fr} (m/s)	V_{rl} (m/s)	V_{rr} (m/s)
Case 1: Straight-line	15	0	Sim.	2.778	2.778	2.778	2.778
			Exp.	2.775	2.775	2.773	2.774
Case 2: Periodic steer	4	15	Sim.	2.768	2.797	2.763	2.804
			Exp.	2.758	2.797	2.756	2.797
	12	-15	Sim.	2.797	2.768	2.804	2.763
			Exp.	2.791	2.777	2.797	2.767
	20	15	Sim.	2.768	2.797	2.763	2.804
			Exp.	2.765	2.799	2.766	2.805

ISSN No:-2456-2165 https://doi.org/10.38124/ijisrt/26may1953

Case 3: Dynamic steer	5	5	Sim.	2.777	2.778	2.777	2.779
			Exp.	2.782	2.772	2.769	2.770
	8	-10	Sim.	2.783	2.775	2.785	2.773
			Exp.	2.784	2.771	2.783	2.778
	11	15	Sim.	2.756	2.828	2.747	2.846
			Exp.	2.757	2.827	2.739	2.845
	14	-20	Sim.	2.887	2.739	2.920	2.723
			Exp.	2.879	2.736	2.927	2.711
	17	25	Sim.	2.739	2.886	2.723	2.919
			Exp.	2.734	2.881	2.722	2.914
	20	-30	Sim.	2.988	2.715	3.033	2.691
			Exp.	2.984	2.723	3.026	2.688

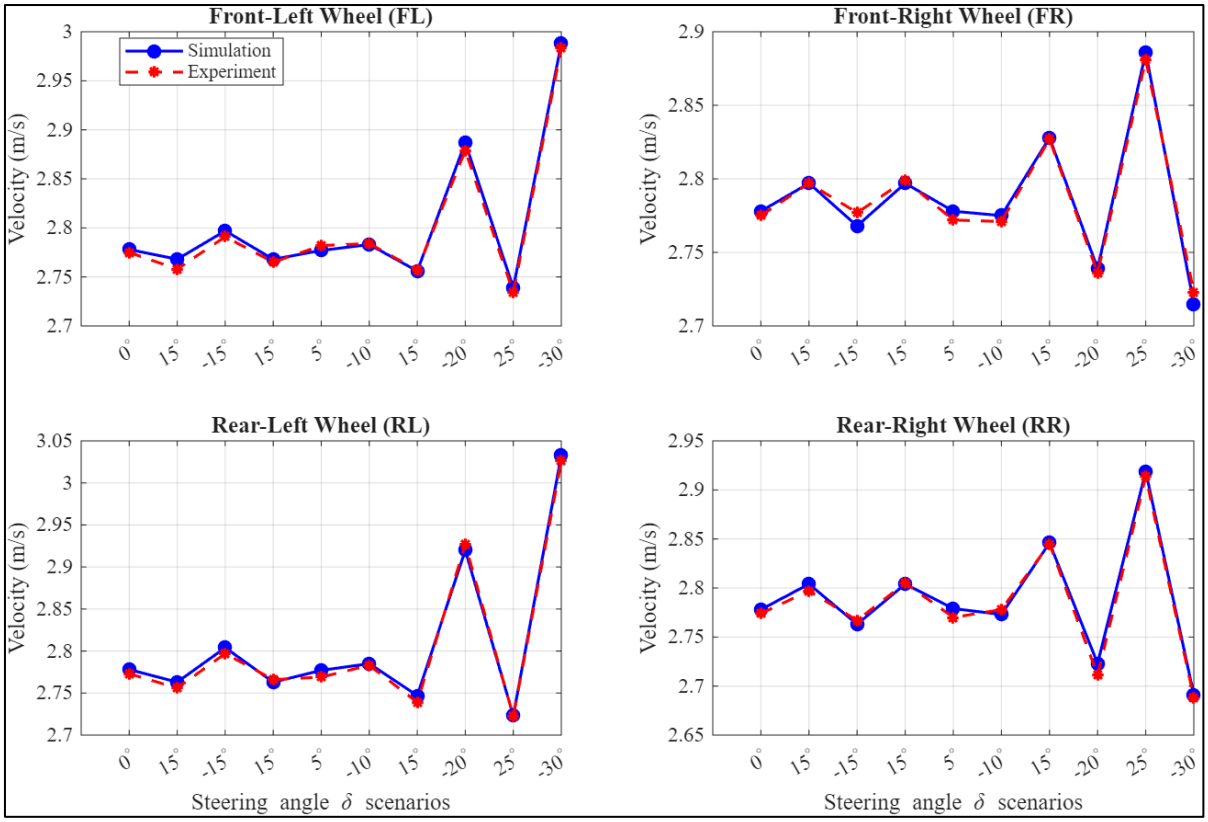

Fig 10 Time-Domain Velocity Tracking Curves Comparing Simulation and Experiment

As illustrated in Fig. 10, a tight correlation is maintained between the theoretical ref-erence trajectories (solid lines) and the empirical feedback data (dashed lines) across all four decoupled driven wheels. Upon receiving a steering command, the physical actuation hardware accurately mirrors the simulation curves, executing dynamic outer-wheel acceleration and inner-wheel deceleration. This confirms the functional fidelity of the embedded Ackermann-based distribution logic under deterministic laboratory conditions.

Minor transient tracking deviations, primarily restricted below a 5% threshold, emerge during rapid steering reversals. These localized errors are attributed to high-order nonlinearities and mechatronic constraints omitted from the idealized kinematic framework, specifically: (i) control loop and signal processing latencies within the microcontroller discretetime execution cycles; (ii) mechanical backlash and compliance within the 1:15 worm-gear steering mechanisms during directional transitions; and (iii) intrinsic internal friction within the hub motor bearing blocks. Nevertheless, the closed-loop PID control structure effectively attenuates these transient disturbances, ensuring steady-state convergence and validating the operational readiness of the developed mechatronic platform.

V. CONCLUSION

This study presented the structural design, kinematic modeling, and laboratory benchtest verification of an electronic differential system engineered for a four-wheel independent steering and four-wheel independent drive mobile robot prototype. By integrating an expanded Ackermann geometric framework with a centralized processing layout utilizing an Arduino Mega board and dedicated motor drives, a flexible locomotive testing platform was successfully constructed.

The comparative analysis between the MATLAB/Simulink numerical environment and the experimental sensor data validated the baseline tracking capabilities of the control loop architecture. The embedded

ISSN No:-2456-2165 https://doi.org/10.38124/ijisrt/26may1953

electronic differential mapping successfully allocated localized velocity commands to each driven wheel proportional to the active steering inputs. The velocity tracking errors between the simulation references and the no-load bench test feedback were maintained below 5% across diverse steering profiles spanning from 5^o to 30^o, demonstrating that the individual drive loops possess sufficient bandwidth to track the kinematic targets effectively under isolated testing conditions.

While the mechatronic prototype and the embedded mapping performed reliably within a controlled laboratory environment, certain research limitations must be acknowledged. The experimental trials were restricted to a no-load bench setup, which isolates the actuation loops but does not account for complex tire-road friction, real-world wheel slip, or terraininduced disturbances. Consequently, the actual effectiveness of the system in preventing lateral tyre scrubbing under active load remains to be verified. Future research phases will focus on deploying the mobile platform in physical field environments to analyze vehicle dynamics under active towing loads. These field data streams will serve as the foundation for developing adaptive control algorithms, implementing Extended Kalman Filters for realtime slip estimation, and integrating spatial sensors to realize a robust autonomous guided vehicle tailored for agricultural monitoring and crop cultivation.

ACKNOWLEDGMENT

This research was fully funded by Tra Vinh University under contract number 432/2022/HD.HDKH&DT-DHTV.

REFERENCES

[1]. Leong JSL, Teo KTK, Yoong HP. Four wheeled mobile robots: A review. 2022 IEEE International Conference on Artificial Intelligence in Engineering and Technology (IICAIET). Kota Kinabalu, Malaysia: IEEE; 2022. p.1-6. https://doi.org/10.1109/IICAIET55139.2022.9936855.

[2]. Pham QP, Huynh DL, Duong VK. Design and experiment of independent Four-Wheel Drive system for electric vehicles. The University of Danang - Journal of Science and Technology. 2026; 24(1):1-6. https://doi.org/10.31130/ud-jst.2026.24(1).616E.

[3]. Zhu S, Lyu C. Distributed Drive Control Technology of Hub Motor. Singapore: Springer Nature Singapore; 2025. https://doi.org/10.1007/978-981-97-2922-7 1.

[4]. Maknickas A, Ardatov O, Bogdevičius M, Kačianauskas R. Modelling the interac-tion between a laterally deflected car tyre and a road surface. Applied Sciences. 2022; 12(22):11332. https://doi.org/10.3390/app122211332.

[5]. Darsh P, Nishi P, Aakash R, Manisha C, Neeraj Kumar GPJ, Cho W. A review on autonomous vehicles: Progress, methods and challenges. Electronics. 2022; 11(14):2162. https://doi.org/10.3390/electronics11142162.

[6]. Yin D, Shan D, Hu JS. A study on the control performance of electronic differential system for four-wheel drive electric vehicles. Applied Sciences. 2017; 7(1):74. https://doi.org/10.3390/app7010074.

[7]. Yin H, Yi W, Wu J, Wang K, Guan J. Adaptive fuzzy neural network PID algorithm for BLDCM speed control system. Mathematics. 2022; 10(1):118. https://doi.org/10.3390/math10010118.

[8]. Yin H, Yi W, Wang K, Guan J, Wu J. Research on brushless DC motor control system based on fuzzy parameter adaptive PI algorithm. AIP Advances. 2020; 10(10):105208. https://doi.org/10.1063/5.0025000.

[9]. Trinh TKL, Nguyen HT, Luu TP. Design of neural network-PID controller for trajectory tracking of differential drive mobile robot. Vietnam Journal of Science and Technology. 2024; 62(2):374-386. https://doi.org/10.15625/2525-2518/18066.

[10]. Thai NH, Ly TTK, Thien H, Dzung LQ. Trajectory tracking control for differential drive mobile robot by a variable parameter PID controller. International Journal of Mechanical Engineering and Robotics Research. 2022; 11(8):614-621. https://doi.org/10.18178/ijmerr.11.8.614-621.

[11]. Kang YH, Pang DC, Zeng YC. Optimal dimensional synthesis of Ackermann steering mechanisms for three-axle, six-wheeled vehicles. Applied Sciences. 2025; 15(2):800. https://doi.org/10.3390/app15020800.

[12]. Zheng H, Yang S, Li B. Optimization control for 4WIS electric vehicle based on the coincidence degree of wheel steering centers. SAE International Journal of Vehicle Dynamics, Stability, and NVH. 2018; 2(3):169-184. https://doi.org/10.4271/10-02-03-0011.

[13]. Gamit P. Simulation of BLDC motor control using conventional PI controller in MATLAB Simulink. Journal of Electrical Systems. 2024; 20(3):8051-8061. https://doi.org/10.52783/JES.7807.

[14]. Dwivedi A. Speed control analysis of BLDC motor drive using PI controller. International Journal of Electrical, Electronics & Communication Engineering. 2013; 3(10):457-462. https://doi.org/10.13140/RG.2.2.35602.96960.

[15]. Mahmud SMA, Motakabber SMA, Alam AHMZ, Nordin AN, Habib AKMA. Modeling and performance analysis of an adaptive PID speed controller for the BLDC motor. International Journal of Advanced Computer Science and Applications. 2020; 11(7):1-8. https://doi.org/10.14569/IJACSA.2020.0110736.